THERMAL MODELLING OF A LOW SPEED AIR-COOLED AXIAL FLUX PERMANENT MAGNET GENERATOR

Y.C. Chong, J. Chick*, M.A. Mueller*, D.A. Staton †, A.S. McDonald #*

** Institute for Energy Systems, School of Engineering, University of Edinburgh, Edinburgh, EH9 3JL, U.K.*
† Motor Design Ltd., 4, Scotland Street, Ellesmere, Shropshire, SY12 0EG, U.K.
 # NGenTec Ltd., 7/9, St. David Street, Edinburgh, EH2 1AW, U.K.

Keywords: AFPM generator, thermal analysis, machine ventilation, Computational Fluid Dynamics (CFD), power loss

Abstract

This paper presents the assessment of air flow in a multi-stage Axial Flux Permanent Magnet (AFPM) prototype which is set to operate at 100rpm. The CFD models are validated using experimental results to give a greater understanding of the air flow developed in the generator. The proposed ventilation design reduces the pressure loss at the entry resulting in a 10% reduction in maximum stator coil temperature in the CFD modelling.

1 Introduction

Direct-drive generators are an attractive proposition for offshore wind energy. Eliminating the gear box significantly reduces the downtime associated with gearbox failure. More recently a novel axial flux permanent magnet (AFPM) generator developed by Mueller and McDonald [1] for wind turbine application has shown a possible reduction in the structural mass by up to 30% compared to convectional permanent magnet generators. Its modular design reduces the cost of manufacture and assembly. Innovation of the machine design offers high power density while high efficiency is maintained for the full operating range. Even for a relatively efficient machine, the high power density can lead to internal heat generation. Excessive temperature in the windings can cause electrical insulation failure and places limits on the maximum rating of electrical machines. Therefore, thermal performance of this low speed air-cooled generator needs to be investigated.

For the AFPM machines, the disc type rotors and stators are oriented in parallel. They form the stator-rotor gaps in the axial direction. During operation, the permanent magnets attached onto the rotor disc act in the same way as radial compressor blades pumping a radial flow out from the machine. Topologies of AFPM generators with short axial length and high power density have gained more attention recently in terms of thermal analysis [2-5]. Convection cooling plays an important role in keeping the generator operating at optimum level. The rate of convection heat transfer is strongly based on the air flow developed in the stator-rotor gap.

The rotating flows in rotor-stator cavities can be found in the literature [6, 7] for turbomachinery. The available literature focuses on the flow structure developed by flat rotating discs. The viscous drag of a rotating surface sets up a swirling flow to move towards the rotating disc. Next to the rotating surface, the tangential flow dominates with a considerable amount of radial outflow. However, the magnet protrusions attached on the rotor complicate the flow structure inside the AFPM machine. Only a limited number of relevant studies have been published [4, 5]. Howey et al. [6, 7] have carried out a useful study on stator convective heat transfer through an experimental investigation for both flat rotor and rotor with protrusions. For a flat rotor, the transition from laminar to turbulent flow begins when the rotational Reynolds number, Re_θ, is greater than 3×10^5 and the flow regime becomes fully turbulent when Re_θ is greater than 5×10^5. However, the transition for a rotor with protrusions is unclear. One might assume that the protrusions encourage turbulent flow and that this occurs at lower Reynolds numbers. This hypothesis is supported by Howey's preliminary experimental results which show higher heat transfer rates. Furthermore, radial inflow at the periphery of the system occurs if the fluid supplied from the entry is less than the fluid leaving the system [8]. The radial inflow further complicates the flow structure in particular at the outer radius, adjacent to the stator surface. This phenomenon depends on the machine ventilation design and the rotational speed.

Figure 1: The 25kW AFPM prototype at the University of Edinburgh

The thermal performance of the low speed air-cooled AFPM generator will be tested to assess ventilation design. The

experimental results will be used to validate the numerical models. Thus, the validated numerical models could provide useful insight to a better ventilation design.

2 Experimental Test Facilities

2.1 Multi-stage AFPM prototype and ventilation design

Figure 1 show a 25kW prototype developed by NGenTec [9]. This is a through flow ventilated machine. The test rig consists of a three stage axial flux generator. The inner and outer diameters of the rotor are 220mm and 460mm respectively. The running clearance between the rotor and stator is 3.5mm providing the gap ratio of 0.0076. The rotor was driven at a fixed speed of 100rpm by means of an inverter fed induction machine through a step down gearbox. The variable speed was not used because the change of ventilation circuit to the air flow in the machine will be assessed. This rotational speed gives the rotational Reynolds number of 1.5×10^5. The motion of the rotor is assumed to create turbulence flow in the stator-rotor gap.

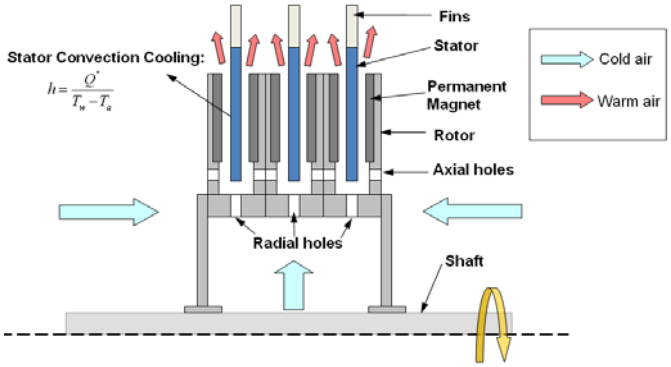

Figure 2: Schematic view of prototype ventilation design

The prototype is naturally cooled with ventilation provided by radial and axial holes on the rotor. A pressure difference is created due to the rotation of rotor. Thus, the surrounding air enters the machine passively through drilled axial and radial holes on the rotor, with one hole per coil in each direction as illustrated in Figure 2. Both axial and radial holes have the same diameter of 20mm. The axial holes are located on a pitch circle radius of 272mm on the rotor side. Four different tests can be performed from this ventilation pattern to analyse their cooling effectiveness.

Case 1: All holes unblocked.
Case 2: Only radial holes unblocked.
Case 3: Only axial holes unblocked.
Case 4: All holes blocked.

The generator is instrumented with thermocouples. These are embedded in the stator to measure the local temperatures on the surface of copper coils. Since the generator is stator-critical, temperature measurement was not performed on the rotor. Also, mechanical difficulties prevent temperature measurement on the rotating parts.

3. Experimental Results and Numerical Models

3.1 Experimental measurements

During tests, the stage of interest (non-driven end stage) was applied with three phase balanced load to match the corresponding mechanical input power of 8.33kW (representing total input power of 25kW for 3 stages). There are 24 coils per stage. The change of temperature of 4 coils of the end stage was monitored using 12 thermocouples. Three thermocouples per coil measured the local temperature at the same some locations (A, B and C) as shown in Figure 3.

Figure 3: Location of thermocouples embedded in the stator

Before the ventilation tests were carried out, the machine was brought up to the steady state operating temperature at full load, requiring two and half hours. The machine was then cooled down for 20 minutes. The machine was run until steady state and the local temperatures of stator coils were recorded as shown in Figure 4 and 5.

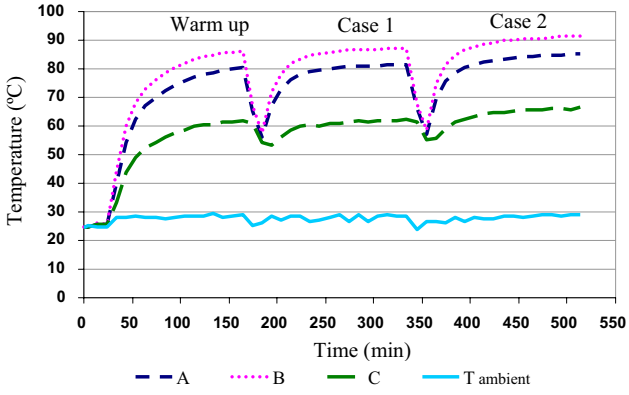

Figure 4: Heating curves of Case 1 and Case 2

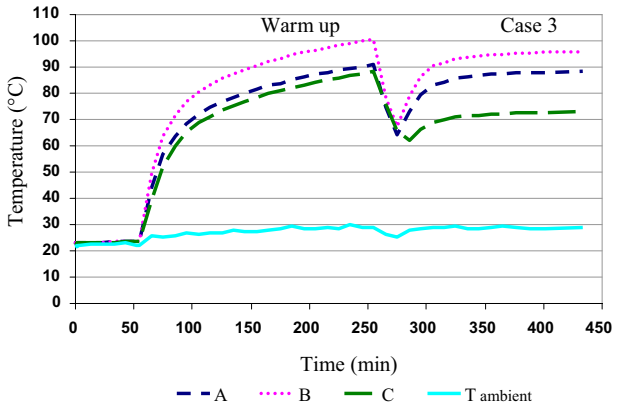

Figure 5: Heating curves of Case 3

Heat generation in a machine depends on the machine energy losses and this causes the temperature rise. Therefore, the energy losses in the generator need to be assessed carefully in order to give an accurate machine operating temperature estimation. The temperature rise is dominated by the copper loss, which is the major loss component in this machine topology. The electrical resistance of copper windings increases linearly with rising temperature. The copper loss in a coil can be defined as:

$$P_{copper} = \left(\frac{I}{n_p}\right)^2 R_{Cu} \qquad (1)$$

I is the total current in a phase, and n_p is the number of coils connected in parallel.

As a result, the phase voltage, phase current and phase power output were monitored and recorded over the entire test period. The electrical resistance (R_{Cu}) of a coil was also measured once steady state was reached.

Eddy current loss also exists in the stator because the changing magnetic field induces circulating currents inside conductors. It is dependent on the square of electrical frequency [10]. The eddy current loss in a coil can be estimated using:

$$P_{eddy} = \frac{\pi^3 B_g{}^2 d_{cond}{}^4 f^2 l_m N_t}{4\rho(1+\alpha\, dT)} \qquad (2)$$

B_g = airgap flux density [tesla, T]
d_{cond} = conductor diameter [m]
f = electrical frequency [Hz]
l_m = radial length of magnet [m]
N_t = number of turns in a coil
ρ = resistivity of copper at ambient temperature [Ω-m]
α = temperature coefficient of resistivity, [K^{-1}]
dT = temperature rise above ambient temperature [K]

Besides eddy current loss, parasitic (circulating) current loss also occurs when a parallel connection is made between the coils in the machine. Since eddy and parasitic current losses are directly proportional to the square of rotational speed, they can be approximated by the quadratic relation [11]. At low speed, the mechanical losses are linearly proportional to the rotational speed. These losses can be determined by no-load tests as:

$$P_{no-load} = K_{parasitic+eddy}\ \Omega^2 + K_{mech}\ \Omega \qquad (3)$$

Ω is the rotational speed, while $K_{parasitic\ +\ eddy}$ and K_{mech} are constants. The input torque was measured using the Magtrol's Torque Transducer TM 315/031 [12] and logged into a computer for post-processing. The input power was fitted to a quadratic function as shown in the equation (3). Then, the parasitic current loss can be determined by subtracting the eddy current loss from the term, $K_{parasitic\ +\ eddy}\ \Omega^2$.

Hence, the heat source in a coil is the sum of copper loss, eddy and parasitic current losses.

$$P = P_{copper} + P_{eddy} + P_{parasitic} \qquad (4)$$

Since the generator was rotated at constant speed, equation (4) is applicable for steady state conditions. As the energy losses in a machine are complex, the scope of this paper only covers the main energy losses in the stator. These energy losses are adequate for the investigation of machine ventilation under steady state conditions.

The generator energy losses determined through experimental measurements are treated as the heat sources in the numerical models. The heat sources for each test case are different because of the change of stator coil temperature under each ventilation circuit.

3.2 CFD models

For the ease of CFD modelling, the three dimensional geometry of generator components were simplified by removing irrelevant design details and modelled using the CAD software, Solid Edge [13]. The modelled components were imported into a STAR-CCM+'s [14] 3D-CAD model for some modifications to form the specific CFD geometry. The material covering stator coils is epoxy, and this region is formed by extracting the internal volume from stator fins and coils in the 3D-CAD model. In addition to this, the fluid regions were created representing the fluid domain of rotor-stator cavities and machine surroundings.

Only 1/8 section of a full stage was presented in the study because of the model periodicity and the limitation of computational resources. Thus, a high quality mesh can be generated for this sector. The final CFD model consists of multiple solid and fluid regions. These regions include the coils, epoxy, fins, permanent magnets, rotor and air. Contact interfaces and internal interfaces were created between the regions to specify the conjugate heat transfer and fluid flow.

The STAR-CCM+ meshing tool generated a total number of 1 million polyhedral cells over the regions and prism layer mesher created prism layers in the air region, adjacent to the wall boundaries in order to resolve the turbulence and thermal boundary layers effectively. It is important to note that conformal meshes were preserved on the interfaces during mesh generation. Volume controls were used in the CFD model to provide fine meshes in the rotor-stator cavity.

The air flow simulation was solved by the SST (shear-stress transport) K–ω turbulence model in STAR-CCM+ 6.02. Because of the fluid domain simulation involving thermal conduction and convection, the conservation equations of mass, momentum and energy were solved simultaneously for steady-state flow while only energy equation was solved for solid regions. Two-layer all y+ wall treatment was chosen to solve the near-wall turbulent boundary layers. However, the wall y+ (non-dimensional distance from the wall to the centroid of the wall-adjacent cells) was set to be less than 1 to resolve viscous-affected region of the boundary layers. The cooling air was assumed to be an ideal gas. The air properties (dynamic viscosity, specific heat, thermal conductivity and turbulence Prandtl number) are constant throughout the simulation, as these properties do not change very much during the simulation and have insignificant effect on the simulated solutions.

The Moving Reference Frame (MRF) approach was used to model the motion of the rotor for time-averaged steady-state solutions. This assumes the buoyancy effect can be neglected. The sliding mesh approach needs to be employed to provide a time-dependent solution if the buoyancy effect is to be taken into account, but the computational cost is significantly higher.

3.3 Validation of CFD models

Convective heat transfer dominates the cooling process of the generator. The presence of bulk air motion brings the undesired heat out of the generator. Advances in CFD analysis allow detailed evaluation and prediction of air flow for the corresponding ventilation circuit. By incorporating the generator energy losses from experimental measurements, the CFD models were validated through the comparison of temperature distribution.

Based on the CFD simulations, the air entering the machine circulates in the rotor-stator gap in the tangential direction. Meanwhile, the cooling air is pumped out of the generator radially due to the pumping effect caused by the rotor. The prediction of flow rates of cooling air through the ventilation holes of the stage tested are presented in Figure 6.

The change of flow rate passing through the generator changes the level and distribution of convective cooling since the cooling effectiveness is strongly dependent on the bulk motion of air. The comparison of stator coil temperature between the experimental measurements and CFD predictions is tabulated in Table 2.

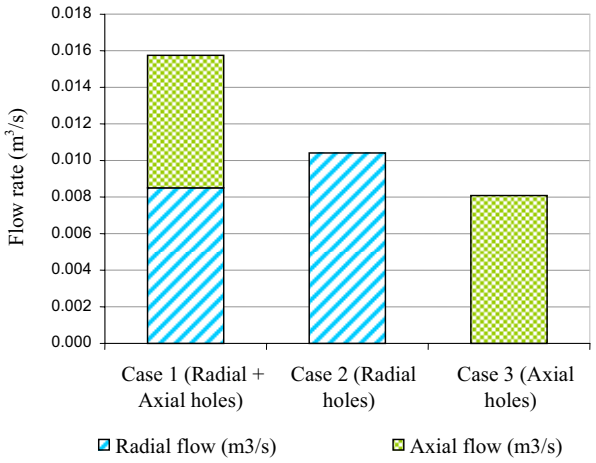

Figure 6: Flow rate of ventilating air of the stage tested

Ventilation Circuit	Method	Temperature			Max. Error (%)
		A (ºC)	B (ºC)	C (ºC)	
Case 1	Experiment	81.6	87.2	62.2	12.2
	CFD	78.1	81.1	69.8	
Case 2	Experiment	85.4	91.4	66.8	15.1
	CFD	83.8	87.6	76.9	
Case 3	Experiment	88.5	96.0	73.1	19.6
	CFD	95.0	99.3	87.4	
Case 4	Experiment	–	–	–	–
	CFD	144.7	151.0	151.9	

Table 2: Comparison of experimental and CFD simulation temperature

The comparison between experimental measurements and CFD predictions shows good agreement. Case 1 with all ventilation holes unblocked shows the best cooling performance. This is supported by the flow rate of ventilating air. The higher the flow rate, the lower the stator coil temperature. As the stator coils generate the principal heat, the stator surface has a higher temperature in particular around where the copper coils placed. Coil temperature "loops" can be clearly seen in Figure 7.

The temperature measurements of thermocouple A, B and C range between 62.2°C–87.2°C for Case 1, 66.8°C–91.4°C for Case 2 and 73.1°C–96.0°C for Case 3. On the other hand, CFD predictions of the local temperature at A, B and C mostly fall within the range of experimental measurements. CFD estimates the temperature difference between A, B and C are 69.8°C–81.1°C for Case 1, 76.9°C–87.6°C for Case 2 and 87.4°C–99.3°C for Case 3. For Case 3 with only axial ventilation holes, the maximum temperature predicted in the CFD is 3.4% out of the measured temperature range.

The stator coils are the active parts of the generator. They have the hottest temperature. Thermocouple B recorded the highest temperature because it is located in the middle of stator coil in the radial direction. Lower temperatures were recorded by thermocouple A and C because the aluminium

fins are placed at the outer edge of stator coils and the impingement of incoming air cools the inner radius of stator coils considerably.

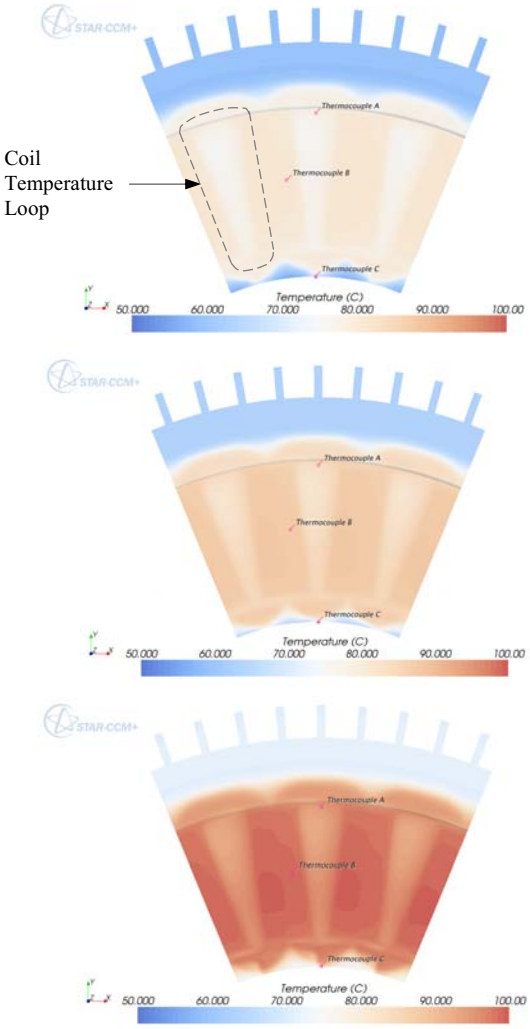

Figure 7: Temperature contour of stator surface for Case 1, Case 2 and Case 3 respectively

It was not possible to reach the steady state condition for Case 4 because of the risk of overheating. The maximum thermocouple reading was over 100°C and it kept rising. The blockage of all ventilation holes completely change the flow field developed in the generator. With respect to mass conservation, both radial outflow and inflow occur at the outer radii of stator-rotor gap. The radial outflow is adjacent to the rotor surface, whereas the radial outflow is adjacent to the stator surface as shown in Figure 10. Hence, Case 4 has different stator temperature distribution compared to above ventilation tests. Since the steady state condition was not reached, the heat sources of Case 1 are used for CFD modelling. CFD shows the hot-spots are located at the inner radius of stator (about 153ºC). The temperature measurement of thermocouple C of Case 4 shows much higher values compared to Case 1–3, which is closer to the temperature reading at point B. This is agreed with the experimental measurements as shown in Figure 8.

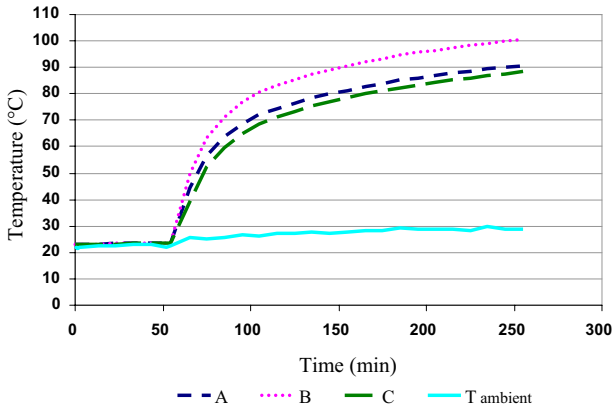

Figure 8: Heating curves of Case 4

One should notice that the experimental tests show wider range between the maximum and minimum temperatures, while the temperature ranges of the CFD prediction are smaller. The temperature difference in experiment between B and C is 19.4°C for Case 1, 24.6°C for Case 2 and 22.9°C for Case 3 whereas the temperature difference in CFD between B and C is 11.3°C for Case 1, 10.7°C for Case 2 and 11.9°C for Case 3. This situation can be explained. Each stator coil was simplified in the CFD model by a bulk copper region instead of being modelled in detail because it is rather complex. As the materials of insulation and impregnation of windings were not physically modelled, the conduction thermal resistance (m^2-K/W) due to the insulation and impregnation materials is expressed as:

$$R_t = \sum_{i=1}^{n} \frac{l_i}{k_i} \qquad (5)$$

l is the thickness of insulation and impregnation, k is the effective thermal conductivity and n is the number of winding layers. The thermal resistance was applied as the contact resistance of the interfaces between copper and epoxy regions. Consequently, the CFD model has a steep change in temperature across the contact interface. However, the actual generator exhibits a gradual gradient from the hot-spot locations to the stator surface. In addition to this, the discrepancy might be caused by the obstruction of bundles of measuring cables and wires at the generator periphery as shown in Figure 1 that restricting the radial outflows as they are not modelled in CFD.

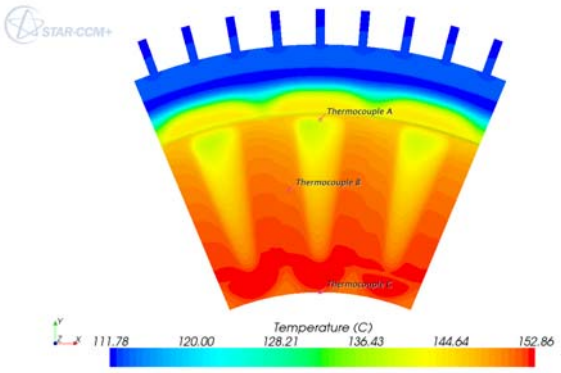

Figure 9: Temperature contour of stator surface for Case 4

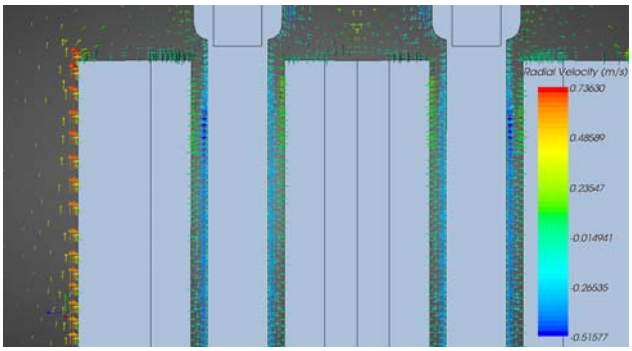

Figure 10: Flow field of Case 4 modelled using CFD

Energy losses at the rotor such as magnet loss were not taken into account in the thermal analysis. Hence, the CFD simulations assume larger temperature difference between stator and rotor and this will over-predict the heat transfer rate. However, this influence is weak because the energy losses at the rotor are rather small for the generator.

4. Discussion

Heat generated in a generator results in a temperature rise throughout the machine. Accurate temperature estimation can be achieved with accurate air flow modelling. Numerous models were generated, with each one focused upon a given element of ventilation circuit. The validation of each CFD model is presented in the previous section. Thus, the cooling effectiveness could be evaluated from the aid or obstruction of the corresponding elements to the machine ventilation.

According to [4], the size of the air inlet is very important in determining or limiting the flow rate of air through the through flow ventilated machine. In theory, the abrupt change in flow cross sectional area will considerably increase the pressure drop. In fact, the fluid flow has negative effect to the pressure drop. High pressure drop gives low flow rate in a system. Based on this, the entry of the generator is redesigned. The rotor plates of generator are connected by some cylindrical bars and this provides bigger air inlet as illustrated in Figure 11.

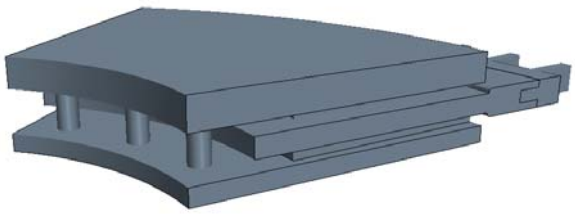
Figure 11: CAD geometry of proposed ventilation design

Heat sources of Case 1 were applied to the CFD analysis. The proposed ventilation design shows an improvement of cooling effect. The fully opened system reduces the pressure drop at the entry and allows more air passing through the generator. CFD gives an estimation of 0.0258m^3/s of cooling air through a single stage which is 64% higher than Case 1. The maximum stator coil temperature is below 73ºC, which is about 8ºC (10% reduction) lower than Case 1.

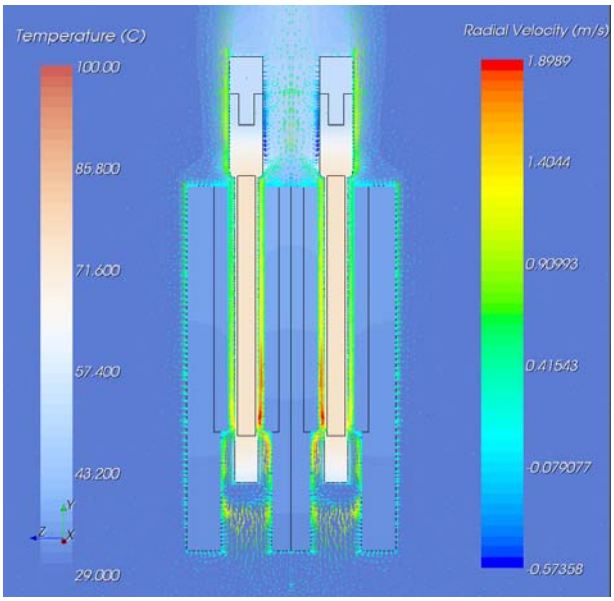

Figure 12: Flow field and temperature distribution of proposed ventilation design

5. Conclusion

Although the generator operates at low rotational speed, the thermal analysis in this paper shows that the direct-drive AFPM generator can still achieve effective cooling. This can provide gains in power output. Incorporation of experiment and CFD analysis has provided a greater understanding to the flow field developed in the generator from its ventilation pattern. From this study, the following conclusions can be made:

- The air flow rate through the generator determines the cooling effectiveness. Good cooling performance can be achieved by optimizing the ventilation circuit to minimise the pressure drop in the system.

- The most effective cooling is achieved by designing the ventilation system such that there is a continuous flow of air across the coils, most easily achieved by inducting cool air at the inner radii and exhausting to the outer radii. Therefore, the occurrence of both radial outflow and inflow at the outer radius of the stator-rotor gap needs to be avoided.

- Since the flow path of the generator is orientated in the radial direction, radial holes allow more air to pass through the machine when compared to axial holes. There are many different configurations of disc type machine. For a through flow ventilated axial flux machine, besides having some ventilation openings at the bottom of the machine, some ventilation openings can be introduced at the side of the rotor to enhance convection cooling. This could be a potential solution for certain disc type machines because of the limited rotor bottom area.

Acknowledgements

The authors are very grateful for the funding, test facilities, advice and support provided by NGenTec Ltd., Motor Design Ltd., Edinburgh University and Energy Technology Partnership (ETP) to the research. The authors would also like to give special thank to E.J.P. Echenique-Subiabre and O.Keysan, who have provided helps to this work.

References

[1] M.A. Mueller and A.S. McDonald, "A lightweight low-speed permanent magnet electrical generator for direct-drive wind turbines," *Wind Energy*, vol. 12, pp. 768–780, (2009).

[2] G. Airoldi, "Numerical Investigations of Air Flow and Heat Transfer in Axial Flux Permanent Magnet Electrical Machines," PhD Thesis, School of Engineering and Computing Sciences, University of Durham, (2010).

[3] Y.C. Chong, D.A. Magahy, J. Chick, M.A. Mueller, A.S. McDonald and D.A. Staton, "Numerical Modelling of an Axial Flux Permanent Magnet Machine for Convection Heat Transfer," 1st International Conference of IET Renewable Power Generation, pp. in-press, (2011).

[4] D. Howey, P. Childs, and A. Holmes, "Air-gap convection in rotating electrical machines," *IEEE Transactions on Industrial Electronics*, pp. in-press, (2010).

[5] D. Howey, A. Holmes, and K. Pullen, "Measurement and CFD prediction of heat transfer in air-cooled disc-type electrical machines," *IEEE Transactions on Industry Applications*, pp. in-press, (2011)

[6] P. Childs, "Rotating flow," 1st edition, Butterworth-Heinemann, (2011)

[7] J.M. Owen, R.H. Rogers, "Flow and heat transfer in rotating-disc systems Volume 2: rotating cavities," 1st edition, Research Studies Press Ltd., (1995).

[8] J.M. Owen, R.H. Rogers, "Flow and heat transfer in rotating-disc systems Volume 1: rotor-stator systems," 1st edition, Research Studies Press Ltd., (1989).

[9] NGenTec. [Online]. Available: www.ngentec.com

[10] G. W. Carter, "The electromagnetic field in its engineering aspects," 1st edition, Longmans, Green and Co, (1954)

[11] J.F. Gieras, M. Wing, "Permanent magnet motor technology: design and applications," 2nd Edition, Marcel Dekker, Inc., (2002)

[12] Magtrol. [Online]. Available: www.magtrol.com

[13] Siemens PLM Software, User Guide Solid Edge Version 20.00.00.96, (2006)

[14] CD-adapco, User Guide STAR-CCM+ Version 6.02.007, (2011)